Article

Hydrogen Storage in Porous Cyanometalates: Role of the Exchangeable Alkali Metal

L. Reguera, J. Balmaseda, L. F. del Castillo, and E. Reguera

J. Phys. Chem. C, **2008**, 112 (14), 5589-5597• DOI: 10.1021/jp7117339 • Publication Date (Web): 18 March 2008

Hydrogen Storage in Porous Cyanometalates: Role of the Exchangeable Alkali Metal

L. Reguera,[†] J. Balmaseda,[‡] L. F. del Castillo,[‡] and E. Reguera*[,§,||]

Universidad de La Habana, Cuba, Universidad Nacional Autónoma de México (UNAM), México, Instituto Politécnico Nacional, México and Universidad de La Habana, Cuba

Received: December 13, 2007; In Final Form: January 30, 2008

The hydrogen storage in zeolite-like hexacyanometalates with different exchangeable alkali metals within the cavities was studied. The H_2 adsorption isotherms were recorded at 75 and 85 K in order to estimate the involved adsorption heats using the isosteric method. The electric field gradient within the porous framework favors the hydrogen adsorption in the materials under study but also could lead to kinetic effects for the pore filling. Such effects were particularly pronounced for sodium among the studied compositions: $Zn_3A_2[Fe(CN)_6]_2$ ($A = Na^+$, K^+, Rb^+, Cs^+) and $Zn_3[Co(CN)_6]_2$. For Na^+, a strong interaction with the H_2 molecule takes place, where appreciable kinetic effects even at 258 K are observed. For $Zn_3[Co(CN)_6]_2$ (rhombohedral phase) where the cavities are free of exchangeable metal and, in consequence, have a weak electric field gradient on their surface, the largest hydrogen storage capacity, close to 12 H_2 molecules per cavity (1.82% by weight), was observed. The hydrogen adsorption in these materials involves adsorption heats in the 6−8.5 kJ/mol range, following the order $K > Rb > Cs \approx Zn_3[Co(CN)_6]_2$. The porous framework of this family of materials is formed by ellipsoidal cavities communicated by elliptical windows. The alkali metals are sited close to the windows. The pore accessibility and pore volume were evaluated from CO_2 adsorption isotherms recorded at 273 K. The free volume was found to be accessible to the CO_2 molecule for all of the studied compositions. According to the obtained isotherms the stabilization of the CO_2 molecule within the pores is caused by the electrostatic interaction between the electric field gradient at the cavity and the adsorbate quadrupole moment. The estimated strength for the guest−host interaction and the accessible pore volume follow the order $Na > K > Rb > Cs$. The largest accessible pore volume was found for $Zn_3[Co(CN)_6]_2$, close to 8 CO_2 molecules per cavity (28% by weight), but with the weaker guest−host interaction. The materials under study were characterized from X-ray diffraction, thermo-gravimetric, infrared, and Mössbauer data. The obtained results shed light on the role of the electric field gradient at the cavity for the hydrogen adsorption.

1. Introduction

The role of greenhouse gas emissions from fossil fuel combustion on the climate changes related to global warming is nowadays well accepted. This fact, together with the increasing energy demand and the progressive decrease for the worldwide reserve of these traditional energy sources, are forcing us to find environmentally compatible alternative energy resources.[1] Related to the clean combustion of hydrogen and its high heating value (572 kJ/mol), the development of an energetic technology based on hydrogen appears to be one of the most promising options, particularly for vehicular applications.[2] In that sense, the main fundamental and technological challenge is to find an appropriate method for molecular hydrogen storage, with high gravimetric capacity, of at least 6 wt %, and fast adsorption−desorption kinetics at temperatures below 373 K.[3] The highest hydrogen storage capacity has been reported through the use of chemical and metal hydrides but, with these materials, the hydrogen desorption usually requires high temperatures (>500 K) and reversibility is not always guaranteed.[3] These features are the main handicap of these storage media. An attractive option is the physical adsorption due to its reversibility, but with the inconvenience, to date, of relatively low gravimetric density of adsorbed hydrogen.[4] Several families of porous materials have been evaluated for hydrogen storage, among them, carbon-based materials,[5] zeolites,[6] and metal-organic frameworks.[7−9] For zeolites, the presence of exposed highly polarizing cations in channels and cavities has been related to the possibility of attaining appropriate stabilization for the hydrogen molecules within the microporous structure.[4,6,10] More recently, porous coordination polymers, of Prussian-blue type, have received certain attention as prototypes of materials for hydrogen storage.[11−16] The relatively high ability that these materials show for hydrogen storage has been attributed to the availability of free coordination sites for the nitrogen-bound metal sited at the pore's surface, in their anhydrous phases.[11−16] However, the role of the pore surface electric field gradient for the hydrogen storage remains to be clarified. A high electric field gradient could favor a higher excess for the hydrogen molecule within the cavity but also could be contributing to reduce the hydrogen diffusion rate through the porous framework delaying the cavities filling. The role of the alkali metal sited within the pore for the hydrogen adsorption has been explored in alkali metal exchanged zeolites,[4,6,17] but not for porous coordination polymers. In this contribution, we are reporting the hydrogen adsorption in a family of porous hexacyanometalates, $Zn_3A_2[Fe(CN)_6]_2$, where

* To whom correspondence should be addressed. E-mail: ereguera@yahoo.com.

[†] Facultad de Química.

[‡] Departamento de polímeros, Instituto de Investigaciones en Materiales, Universidad Nacional Autónoma de México, México, D.F. C.P. 04510.

[§] Instituto de Ciencia y Tecnología de Materiales.

[||] Centro de Investigación en Ciencia Aplicada y Tecnología Avanzada-Unidad Legaria.

10.1021/jp7117339 CCC: $40.75
Published on Web 03/18/2008

TABLE 1: Formula Unit, Dehydration Temperature, Unit Cell Parameters, ν(CN) Frequency, and Mössbauer Isomer Shift (δ) for the Materials under Study

formula unit	dehyd. *T*, [K]	cell parameters[a] [Å]	ν(CN), [cm^{-1}]	δ[b] [mm/s]
$Zn_3Na_2[Fe(CN)_6]_2.8.9H_2O$	473	$a = b = 12.4787(7)$ $c = 32.906(3)$	2101	0.18
$Zn_3K_2[Fe(CN)_6]_2.6.8H_2O$	436	$a = b = 12.5409(3)$ $c = 32.158(1)$	2100	0.18
$Zn_3Rb_2[Fe(CN)_6]_2.6H_2O$	390	$a = b = 12.5013(2)$ $c = 32.512(1)$	2101	0.18
$Zn_3Cs_2[Fe(CN)_6]_2.5.6H_2O$	370	$a = b = 12.4841(3)$ $c = 32.832(4)$	2100	0.19
$Zn_3[Co(CN)_6]_2$-R		$a = b = 12.4847(3)$ c: 32.756(1)	2203	

[a] In a hexagonal representation. [b] Isomer shift values are given relative to sodium nitroprusside; fitting error in δ remains below 0.01 mm/s.

the framework metal coordination environment remains saturated with atoms from the CN bridges but with different exchangeable cations (A = Na^+, K^+, Rb^+, Cs^+), including a composition free of exchangeable metal ion, $Zn_3[Co(CN)_6]_2$, which has a weaker electric field gradient at the cavity surface and greater available space. Such a family of hexacyanometalates serves as a prototype of the porous solid, where the electric field gradient within the porous framework can be modulated by the charge balancing (exchangeable) cation. The obtained results help to shed light on the role of the porous framework electric field gradient for the hydrogen storage in porous materials.

The crystal structure of the materials under study is known.[18,19] They crystallize with a rhombohedral unit cell (R-3c space group) related to a tetrahedral coordination to the N end of the CN group for the zinc atom, while the inner metal (Fe, Co) preserves its usual octahedral coordination to the C end with a low spin electronic configuration.[19,20] Their network of pores is formed by ellipsoidal cavities of about $12.5 \times 9 \times 8$ Å, three per unit cell, communicated by elliptical opening (windows) of $\sim$5 Å.[18,19] The unit cell contains six formula units.[19] Such cavity geometry has been confirmed by a recent study using ^{129}Xe NMR spectroscopy of adsorbed Xe atoms.[21] The exchangeable cations are sited close to the cavity windows.[18] A detailed discussion for the main structural and thermal features of this family of hexacyanometalates is provided below. Previous to the hydrogen adsorption study, the samples were characterized from X-ray diffraction (XRD), thermogravimetry (TG), infrared (IR), and Mössbauer spectroscopies and CO_2 adsorption data.

2. Experimental Section

Hot aqueous solutions (0.01 M) of zinc chloride and $K_n^+[M(CN)_6]^{n-}$ where M = Fe^{II} or Co^{III}, were mixed, and the resulting precipitate separated after 2 days of aging within the mother liquor at 60 °C. The obtained solid was washed several times with distilled water in order to remove all of the accompanying ions and then dried in air until it had constant weight. For Zn ferrocyanide, the solid precipitated from sodium ferrocyanide was also prepared. The nature of the obtained solids as hexacyanometalates was confirmed from IR spectra. The metals atomic ratio in the studied samples was estimated from energy-dispersed spectroscopy (EDS) analyses, using a spectrometer (from Noran Co.) coupled to a SEM microscope (from Jeol Co.). The hydration degree (number of water molecules per formula unit) was estimated from TG curves. Mixed compositions of Zn ferrocyanides with A = Rb and Cs were prepared through ionic exchange from $Zn_3Na_2[Fe(CN)_6]_2 \cdot xH_2O$ in hot aqueous solutions according to a reported procedure.[22] Zinc cobalticyanide, $Zn_3[Co(CN)_6]_2 \cdot xH_2O$, has been reported as dimorphic, cubic (Fm-3m) and rhombohedral (R-3c).[19] In the following, this last compound will be labeled as Zn_3Co_2-R. The cubic phase is usually obtained from the synthesis at room temperature, whereas the rhombohedral one is formed from hot solutions or on dehydration of the cubic phase by heating above 60 °C.

A high-resolution TA Instrument (Hi-ResTM) thermo-gravimetric analyzer TGA 2950 and instrument control software Thermal Advantage version 1.1A were used to measure the weight loss profiles for the studied samples. The TGA 2950 was used in dynamic rate mode where the heating rate is varied dynamically according to a ramp in response to the derivative of weight change (as the derivative increases, the heating rate is decreased, and vice versa). The heating rates were constrained to be at the 0.001 to 5 °C/min range with an instrumental resolution of 5. The furnace purge was nitrogen using flow rates of 100 mL/min. IR spectra were collected using a FT−IR spectrophotometer (Spectrum One, from Perkin-Elmer) and the KBr pressed disk technique. Mössbauer spectra were recorded at room temperature using a constant acceleration spectrometer operated in the transmission mode and a ^{57}Co/Rh source. The obtained Mössbauer spectra were fitted using a least-squares minimization algorithm and pseudo-Lorentzian lines in order to obtain the values for isomer shift (δ), quadrupole splitting (Δ), and line width (Γ). The value of δ is reported relative to sodium nitroprusside. XRD powder patterns were recorded in Bragg−Brentano geometry by means of a D5000 diffractometer (from Siemens) and monochromatic CuK_α radiation, from 5 to 110 ° (2θ), at a step size of 0.025 and 25 s of counting time.

The CO_2 and H_2 adsorption isotherms were recorded using ASAP 2010 and 2020 equipments (from Micromeritics), respectively. Sample tubes of known weight were loaded with 40−50 mg of sample and sealed using TranSeal. Previous to CO_2 and H_2 adsorption, the samples were degassed on the ASAP analyzer using a heating rate of 1 °C/min and then maintained at the dehydration temperature indicated by the TG curve to obtain a stable outgas rate below 1 μHg. The degassed sample and sample tube were weighed and then transferred back to the analyzer with the TranSeal preventing exposure of the sample to air. After volume measurement with He the degassing was continued for 24 h at 80 °C in the sample port. Measurements were performed at 273 K for CO_2 using an ice−water bath and at 75 and 85 K for H_2 using liquid N_2 and Ar baths. These relatively low temperatures for liquid N_2 (75 K) and Ar (85 K) are related to the local atmospheric pressure, 586 Torr. For Na, the H_2 adsorption isotherm was also recorded at 258 K.

The CO_2 adsorption data were evaluated according to the Dubinin−Astakhov (DA) equation:[23]

$$n_{ad} = n_p \cdot \exp\left\{-\left[\frac{RT}{E_0}\ln(P_r^{-1})\right]^n\right\} \quad (1)$$

where n_{ad} is the amount adsorbed at a relative pressure; $P_r = P_{eq}/P_v$, where P_{eq} is the equilibrium pressure, and P_v is the vapor pressure; n_p: the limiting amount filling the micropores; E_0: characteristic energy; n: the heterogeneity parameter; R: the universal gas constant; and T is the temperature. Since the CO_2 adsorption data were collected up to 760 Torr, at a temperature close to the critical temperature for this adsorbate (304 K), the obtained isotherms only contain points for relative pressures below 0.03, far from the saturation region. In such conditions, the correlation between DA model parameters for nonlinear least-squares fitting algorithms leads to non-reliable n_p values. From this fact, the n_p value was estimated using the more general Langmuir−Freundlich (LF) equation based on the vacancy solutions theory:[24]

$$P_{eq} = P_{0.5}\left(\frac{n_{ad}}{n_p - n_{ad}}\right)^g \quad (2)$$

where $P_{0.5}$ is the equilibrium pressure at $n_p/2$, and g is the osmotic coefficient related to ideality of solution and the remaining parameters have the same meaning than in DA equation. Then, once the value of n_p is known, from eq 1, the values of E_0 and n are calculated. Details of this combined application of DA and LF models for the evaluation of adsorption data have been reported elsewhere, including the nonlinear fitting algorithm.[25] The pore volume was estimated multiplying the obtained n_p value by the reported molar volume for liquid CO_2 (42.9 mL/mol).[26]

Within the DA model formalism, the adsorption potential can be estimated directly from the obtained adsorption isotherm according to:[23]

$$A = RT\ln(P_r^{-1}) \quad (3)$$

The hydrogen adsorption isotherms were evaluated according to eq 2 to estimate the limit capacity of micropores (np) and the osmotic coefficient (g) value. As will be discussed, the value of g can be used as sensor for the strength of the guest−host interaction. The enthalpy of adsorption (ΔH_{ads}) was obtained by the isosteric method from isotherms recorded at N_2 and Ar baths and then using a variant of the Clasius−Clapeyron equation to calculate the ΔH_{ads} value according to the following:[27]

$$\ln\left(\frac{P_1}{P_2}\right) = \frac{\Delta H_{ads}}{R}\frac{T_2 - T_1}{T_1 \cdot T_2} \quad (4)$$

3. Results and Discussion

3.1. Structural and Thermal Characterization of the Samples to be Studied. The atomic metals ratio estimated from EDS analyses corroborated the expected nominal formula units, $Zn_3A_2[Fe(CN)_6]_2 \cdot xH_2O$ (A = Na, K, Rb, Cs) and $Zn_3[Co(CN)_6]_2 \cdot xH_2O$. In the following, the ferrocyanides series will be labeled as $Zn_3A_2Fe_2$. The obtained XRD powder patterns correspond to a rhombohedral unit cell (R-3c space group), which agrees with the reported crystal structure for A = Na, K, Cs[18,22,28] and also for the cobalt analogue.[19] In Table 1, the calculated unit cell parameters are summarized. The ν(CN) band frequency in the IR spectra of hexacyanometalates is a good sensor for valance, electronic configuration, and coordination number for the metals linked at the C and N ends of the CN ligand. For rhombohedral zinc ferrocyanides, this vibration was observed around 2100 cm^{-1} (Table 1), independently of the involved alkaline metal. The alkaline metal is a charge balancing ion, with only an electrostatic-type interaction with the solid framework. For zinc cobalticyanide, this vibration was observed at 2203 cm^{-1}, coinciding with reported IR spectra for the rhombohedral modification of this compound.[19] Mössbauer spectra of zinc ferrocyanides are single lines with a low isomer shift (δ) value, typical of low spin Fe(II) (Table 1). The iron (II) atom is sensing a highly symmetric charge environment since no quadrupole moment-electric field gradient interaction from the obtained Mössbauer spectra was detected. For the zinc ferricyanide analogue, with also a rhombohedral (R-3c) structure, the reported spectrum is a quadrupole doublet of very low quadrupole splitting value (Δ = 0.18 mm/s) indicating that the iron (III) atom is sensing a weak electric field gradient at its charge environment.[20,25] In those porous hexacyanometalates where the hydrogen adsorption has been reported,[11−13,15,16] the metal (T) bounded to the nitrogen atom is always found at the pore surface with a mixed and distorted coordination sphere, $TN_{6-x}(H_2O)_x$.[20,25] When the crystal water is removed the coordination environment for this metal becomes unsaturated, inducing a higher local distortion and a stronger metal−metal interaction through the CN bridge. For ferricyanides, such an effect is detected as a variation for both δ and Δ values. The increase for the metal−metal interactions leads to a smaller δ value while the higher local distortion is detected as a larger value of Δ.[29]

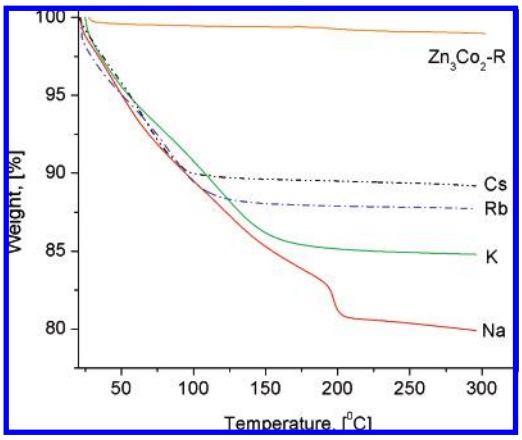

Figure 1. TG curves (dehydration region) for the materials under study: $Zn_3A_2[Fe(CN)_6]_2 \cdot xH_2O$, A = Na, K, Rb, Cs; and $Zn_3[Co(CN)_6]_2$ rhombohedral phase (Zn_3Co_2-R).

Figure 1 shows the TG curves for all of the studied samples. Zinc cobalticyanide was found to be anhydrous. It seems that the surface adsorption potential at the pore surface for this compound is insufficient to produce an excess of water molecules within the porous framework. The de-hydration temperature for zinc ferrocyanides, taken at the end of the de-hydration process, parallels the reported polarization power for the involved exchangeable cations (Na > K > Rb > Cs).[30] These metal ions remain hydrated and their coordination waters are the last ones to be liberated. The pores contain additional waters, of zeolitic nature, hydrogen bonded to the coordinated ones, probably forming water clusters. These weakly bonded water molecules abandon the solid at relatively low temperature in a practically continuous process (Figure 1). Once the first zeolitic waters are removed, the remaining ones enhance their mutual interactions and a higher temperature is required to allow their release. This could explain the observed continuous weight loss for the TG curves. The materials under study, in their anhydrous form, remain stable up to above 300 °C.

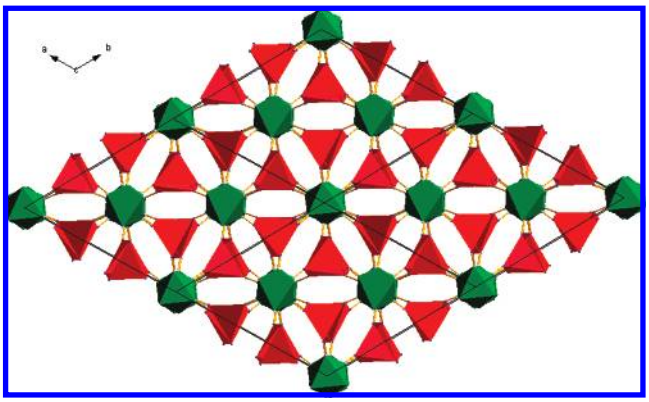

Figure 2. Porous framework (excluding the exchangeable alkali metal) for the materials under study. Relatively large ellipsoidal cavities remain communicated by elliptical windows, six per cavity.

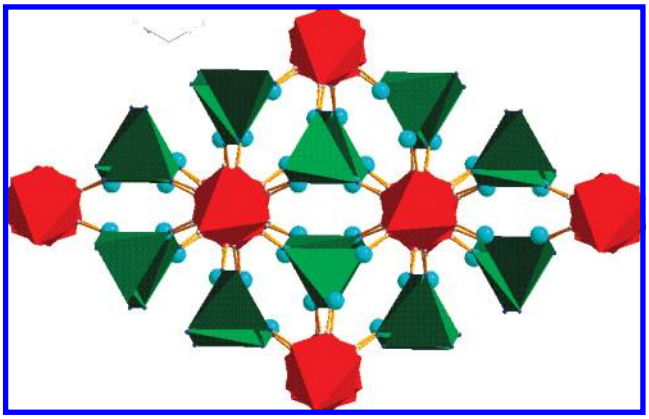

Figure 3. Framework of the materials under study. The exchangeable alkali metals located close to the ZnN_4 polyhedron corners are indicated with small spheres. That position for the alkali metal corresponds to the estimated coordinates for the hydrated material. From the recorded CO_2 and H_2 adsorption data evidence for the cation mobility on the cavity filling was obtained.

3.2. Porous Framework. Figure 2 shows the porous framework of the materials under study represented as the assembling of MC_6 octahedra and ZnN_4 tetrahedra. The synthesis process really corresponds to the assembling of octahedral anionic blocks, $[M(CN)_6]^{n-}$, through Zn^{2+} cations which link neighboring blocks at the N ends. In Prussian blue analogues (cubic Fm-3m) where both the inner and outer metals are found with octahedral coordination, the M−C≡N−T−N≡C−M chain remains practically linear, and the pore window has a square cross section.[21,25] In the R-3c structure, the M−C≡N bond remains practically linear but the N−Zn−N one deviates from the linearity.[18−20] On average, in the materials under study, the N−Zn−N angle was estimated to be 108°. The formation of windows of elliptical shape and also of ellipsoidal cavities is related to such deviation from linearity. This local deformation around the Zn atom, together with the excess of negative charge from the anion, is probably responsible for certain concentration of electric field gradient close to the pore windows since the charge balancing cations in zinc ferrocyanides are found close to the windows.[18,19] Figure 3 shows that the alkali metal is located close to the ZnN_4 corners. As already-mentioned, the Mössbauer spectrum for the studied ferrocyanides, which senses the charge environment due to the first neighbors for the iron atom, is a single line (Table 1). During the synthesis process, the $[M(CN)_6]$ block practically preserves the octahedral geometry. This is also supported by the IR spectra for this family of compounds where the F_{1u} motion for the CN group remains

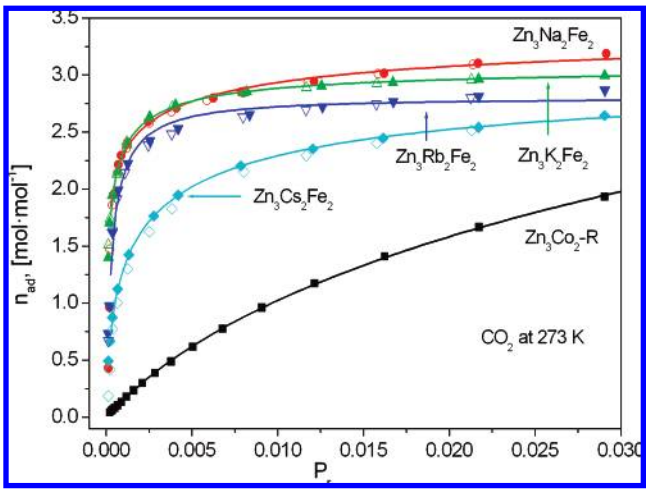

Figure 4. CO_2 adsorption isotherms at 273 K for the materials under study: $Zn_3A_2[Fe(CN)_6]_2$, A = Na, K, Rb, Cs; and $Zn_3[Co(CN)_6]_2$ rhombohedral phase (Zn_3Co_2-R).

degenerated (a single absorption band).[19] The deviation of the M−C≡N−Zn−N≡C−M chain from the linearity for the rhombohedral structure finds conclusive evidence in the magnetic properties of zinc ferricyanide.[20] In the cubic phase of this compound, the Fe^{III} ions appear separated at a distance of 10.2 Å, and its Curie−Weiss ($|\theta_{CW}|$) constant is 5.1(1) K, whereas in the R-3c structure, where these ions are found to be at shorter distance between them, 7.4 Å, this parameter ($|\theta_{CW}|$) results 3.1(1) K. This is equivalent to a weaker magnetic interaction between the iron atoms for the R-3c phase. In this last structure, the overlapping path between the unpaired electrons on neighboring iron atoms results unfavorable. In addition to the structural studies,[18,19] the ellipsoidal geometry for the cavity in the materials under study has been confirmed by ^{129}Xe NMR spectroscopy.[21]

3.3. Carbon Dioxide Adsorption Isotherms. Carbon dioxide is a linear molecule with a relatively small effective cross section along the O−C−O axis, which facilitates its diffusion through small windows and narrow channels. CO_2 is a quadrupolar molecule sensible to the cavity electric field gradient, a behavior also expected for H_2. From this fact, the obtained results from CO_2 adsorption contributes to shed light on the driving force for the hydrogen molecule stabilization in the materials under study. The CO_2 adsorption isotherms were also used to shed light on the alkaline metal effect on the pore accessibility. The alkaline metal atoms sited close to the pore windows could be a limiting factor for the pore filling. From this fact, the CO_2 adsorption experiments were carried out at 273 K, only 31 K below the CO_2 critical temperature. At the used measurement temperature (273 K), the CO_2 molecule has sufficient kinetic energy to diffuse through small windows. Figure 4 shows the collected CO_2 adsorption isotherms. According to these isotherms, in ferrocyanides the electric field gradient at the cavity notably enhances the CO_2 adsorption. At relatively low pressures, the adsorption isotherm shows saturation, suggesting that all of the available free volume has been occupied by CO_2 molecules.

Previous adsorption studies in porous cyanometalates have proven the usefulness of the DA model to evaluate the CO_2 adsorption data,[25,29,30] alone or in combination with the LF model,[25,30] and in correspondence with that information, the CO_2 isotherms obtained for the studied series of zinc hexacyanometalate-based materials were evaluated using the combination of both DA and LF models. The estimated parameters values

TABLE 2: Results Derived from the CO_2 Adsorption Isotherms Fitting According to the Dubinin−Asthakov Model[a,b]

compd	E_0, [kJ/mol]	n_p, [mol/ mol]	n	CO_2/ Cavity	wt %	V_p, [cm^3/g]	g^a
$Zn_3Na_2Fe_2$	23.1 ± 0.6	3.37 ± 0.09	2.5 ± 0.3	6.74	22.3	0.217 ± 0.006	4 ± 1
$Zn_3K_2Fe_2$	22.0 ± 0.1	3.048 ± 0.02	3.9 ± 0.1	6.1	19.2	0.187 ± 0.001	3.1 ± 0.6
$Zn_3Rb_2Fe_2$	19.5 ± 0.01	2.96 ± 0.04	5.9 ± 0.5	5.9	15.5	0.152 ± 0.002	2.4 ± 0.4
$Zn_3Cs_2Fe_2$	16.81 ± 0.04	2.76 ± 0.02	2.87 ± 0.03	5.6	14.7	0.144 ± 0.001	2.0 ± 0.2
Zn_3Co_2−R	8.2 ± 0.2	3.96 ± 0.06	2.0 ± 0.05	7.9	28	0.346 ± 0.001	1.059 ± 0.003

[a] n_p, the limiting amount adsorbed filling the micropores; E_0, characteristic energy; n, heterogeneity parameter; V_p, pore volume; and storage capacity in weight percent (wt %). [b] Value obtained for the osmotic coefficient (g) from the CO_2 adsorption isotherms fitting according to the LF model.

from the adsorption data fitting are summarized in Table 2. The calculated limit amount filling the micropores (Table 2) follows the order Na > K > Rb > Cs. This corresponds to the inverse ordering of these metals according to their ionic radii.[31] For Cs, which is the bigger metal within the considered series, the CO_2 adsorption undergoes a considerable reduction, to about 40% of the observed value for Na (Figure 4, Table 2). Probably Cs, due to its large size (1.85 Å of ionic radius),[31] hinders the accommodation of a significant amount of CO_2 molecules within the cavity. In the obtained isotherm for Cs, no evidence of kinetic effects were observed. The electric field gradient effect on the CO_2 adsorption in the materials under study is evident from a comparison of the obtained isotherms for ferrocyanides with that recorded for zinc cobalticyanide (R-3c) (Figure 4). To Zn_3Co_2-R belongs the isotherm of smaller slope at low adsorption (small n_{ads} values), which corresponds to the weaker interaction for the CO_2 molecule with the cavity. This last compound has the weakest electric field gradient at the cavity, as revealed by its anhydrous character even in a humid atmosphere. It seems that in the studied family of materials, the CO_2 molecule excess within the porous framework is caused by electrostatic interactions without discarding the participation of certain contribution from dispersive forces. Analogue evidence has already been observed for the CO_2 adsorption in porous nitroprussides.[29]

In Table 2, the estimated parameters from the CO_2 adsorption data fitting according to the DA model are summarized. The obtained value for the characteristic energy, E_o, follows the order, Na > K > Rb > Cs > Zn_3Co_3-R, which parallels the expected strength for the electrostatic interaction. For Zn_3Co_2-R, the characteristic energy, E_o, is particularly low, 9.23 ± 0.47 versus 22.7 ± 0.4 kJ/mol for sodium-zinc ferrocyanide (Table 2). In the DA model, the E_o value senses the average strength for the guest−host interaction during the adsorption phenomenon. An analogue result is obtained from the adsorption potential (A), calculated according to eq 3, except for sodium (Figure 5). For low values of the fractional pore filling ($\theta = n_{ads}/n_p$), where the contribution of the guest−guest interaction to the adsorption process is minimized and could be ignored, the adsorption potential follows the order K > Rb > Cs > Zn_3Co_3-R, similar to that already inferred from the calculated E_o values. For Na, the estimated value for the adsorption potential at low θ values cannot be fitted according to eq 3. This reveals a certain unique behavior for this ion, which is more pronounced for the hydrogen adsorption (discussed below). Probably, the relatively strong interaction of the CO_2 molecule with the sodium ion facilitates a greater mobility of this last one within the cavity and to a more pronounced variation for the adsorption potential.

According to the estimated amount filling the micropores, in mol/mol, a cavity free of alkaline metal is occupied by practically 8 CO_2 molecules. This is equivalent to 28 wt % of CO_2 storage capacity in Zn_3Co_3-R. In the structure of the materials under study, there are two formula units per cavity. Probably, this relatively large amount of CO_2 molecules adsorbed per cavity is related to the geometry of both adsorbate and available free volume in the host solid. In the studied ferrocyanides, a fraction of that free volume is occupied by the alkali metal and the estimated amount filling the micropores follows the order Na > K > Rb > Cs (Table 2). For Cs, close to four CO_2 molecules can be accommodated within a cavity. The observed value for the heterogeneity parameter (n) suggests that the CO_2 molecule is sensing certain variation for the adsorption potential within the cavity on the pore filling. Such variation could be related to the alkali metal mobility, a well-known and studied phenomenon in zeolites.[33] For Zn_3Co-R, the obtained value of 2 for n is an expected result. The cavity surface for this material is practically free of electric field gradient, similar to porous carbons whose isotherms are usually fitted with $n = 2$ in DA model.[23]

3.4. Hydrogen Adsorption Isotherms. Figure 6 shows the obtained hydrogen adsorption isotherms at the nitrogen bath. The slope of these adsorption curves is particularly pronounced at low values of pressure suggesting that the hydrogen molecule is participating of a relatively strong guest−host interaction at the cavity. The strength of that interaction, taken as the slope for the adsorption isotherm at low values of pressure, follows the order K > Rb > Cs > Zn_3Co-R (Figure 7). The exception appears to be the sodium-containing ferrocyanide (also discussed below). This order parallels the polarizing power for these three metals (K, Rb, Cs),[33] a behavior similar to that discussed above for the CO_2 adsorption. Compared to CO_2, the hydrogen molecule has a smaller quadrupole moment;[34] however, H_2 is a molecule with only two protons in its nucleus and probably with certain ability to be polarized in the presence of a strong electric field. An analog alkali metal effect on the hydrogen adsorption has been explored from calculations for exchanged zeolites predicting that the embedding of the cations in a zeolite framework causes a dramatic decrease of the polarizing power of the cations.[4,6] The experimental results herein discussed suggest that in zeolite-like hexacyanometalates, the cause for hydrogen molecule excess within the cavity is related to its electrostatic interaction with the cavity electric field gradient, without discarding certain contributions from a direct interaction of H_2 with the metal ion. That first interaction appears to be relatively strong since at 75 K hydrogen is in a supercritical state ($T_c = 32.97$ K), nevertheless, the obtained isotherms show evidence of saturation at medium-pressure values. Since the hydrogen molecule only has a quadrupole moment, such a stabilization within the pores was mainly attributed to a particularly sensitivity of the hydrogen molecule to the electric field gradient. This suggests that the polarizing power of hard ions may provide a means for increasing the interaction of the host materials with the hydrogen molecule.

The hydrogen adsorption in Prussian blue analogues has been attributed to interactions at the pore surface where there are metal centers with unsaturated coordination environment.[11−16] The obtained results for Zn_3Co_2-R discard that correlation

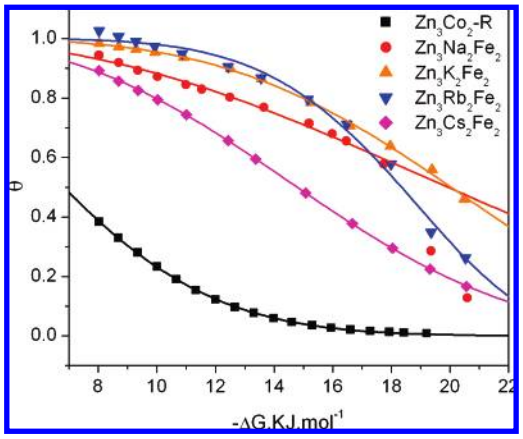

Figure 5. Characteristic curves (experimental and fitted) for the CO_2 adsorption in the materials under study. For low fractional pore filling (θ) where the guest−host interaction predominates the calculated adsorption potential ($-\Delta G$) follows the order Na > K > Rb > Cs > Zn_3Co_2-R.

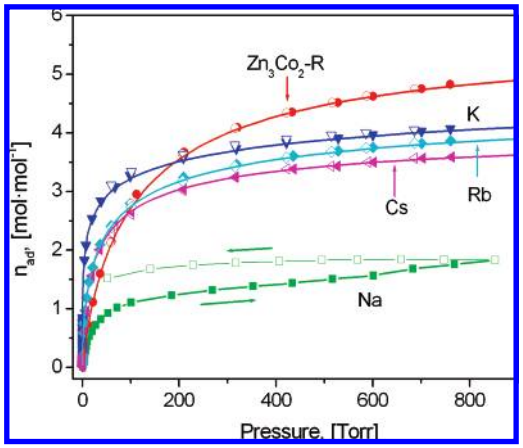

Figure 6. H_2 adsorption isotherms at 75 K for the materials under study: $Zn_3A_2[Fe(CN)_6]_2$, A = Na, K, Rb, Cs; and $Zn_3[Co(CN)_6]_2$ rhombohedral phase (Zn_3Co_2-R).

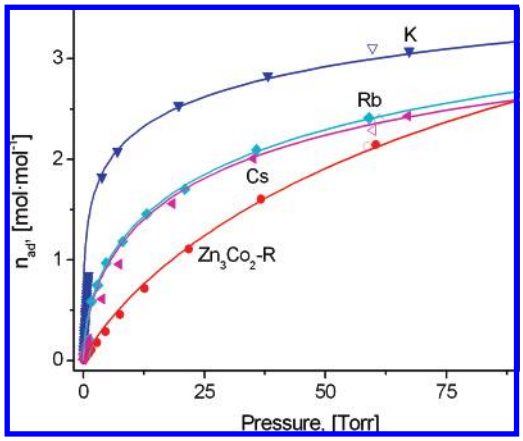

Figure 7. Low pressures region of the hydrogen adsorption isotherms at 75 K for the materials under study, excluding the sodium containing ferrocyanide sample.

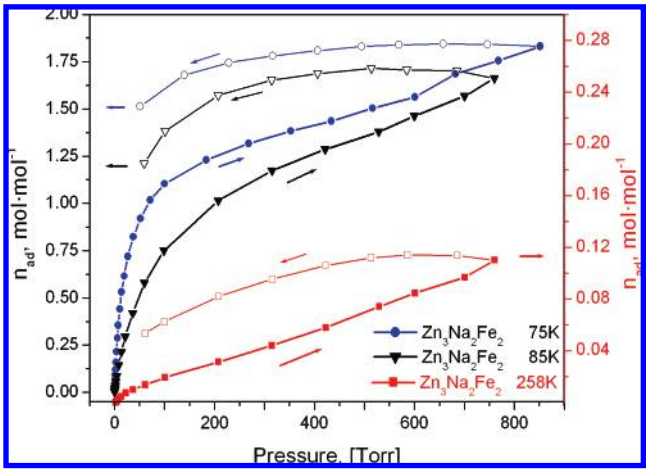

Figure 8. H_2 adsorption isotherms for $Zn_3Na_2Fe_2$ recorded at 75, 85, and 258 K. The kinetic effects are observed even at 258 K. This suggests that a particularly strong interaction between the sodium ion and the H_2 molecule takes place.

because in the structure of this last compound, all of the involved metals have saturated their coordination sphere. It is sufficient that the existence of a certain electric field gradient at the cavity to cause some excess of hydrogen molecules within the pore. In $Cu_3[Co(CN)_6]_2$, a typical Prussian blue analogue with 33.3% of vacancy for the building anionic block, the main adsorption site has been identified to be the interstitial voids, at the 1/4, 1/4, 1/4 crystallographic position.[13] However, in materials with such a large amount of vacancies (cavities), the interstitial sites could also be sensing the electric field gradient from neighboring cavities. For divalent transition metal hexacyanoplatinates (IV) with only interstitial voids as available free space, no hydrogen adsorption has been reported.[12] No hydrogen adsorption has also been observed for anhydrous $Mn_2[Fe(CN)_6]$,[15] a compound with only interstitial free spaces.[35]

When the electric field gradient is strong enough, it could hinder or limit the hydrogen diffusion through narrow windows, which must be appreciated from adsorption isotherms as appearance of kinetic effects. Such effects could also be present when chemical interactions occur during the storage process of the hydrogen molecule. For the case of sodium-zinc ferrocyanide, the observed kinetic effects (Figure 6) were ascribed to a physical interaction. Sodium is the smaller and more polarizing cation within the studied series of exchangeable metals, which favors a strong electrostatic interaction. The obtained adsorption and desorption curves for $Zn_3Na_2Fe_2$ are quite different, even for large measurement times (a week). In this case, the adsorption curve does not correspond to a proper adsorption isotherm because it is recorded under nonequilibrium conditions. A conclusive evidence on the nature of such behavior for the sodium-containing composition as related to kinetic effects was obtained comparing H_2 adsorption isotherms recorded at 75, 85, and 258 K (Figure 8). Even at 258 K, appreciable kinetic effects were observed. The occurrence of a chemical interaction responsible for the observed unique behavior for Na was discarded because at low-pressure, progressive hydrogen desorption takes place. A more detailed study is required in order to understand the nature of that behavior for sodium. At the opposite side, Zn_3Co_2-R is found. This last compound has the largest pore window size and the weaker electric field gradient at the cavity for the studied family of materials. In this compound, the adsorption isotherm is recorded in relatively short time (4 h, including desorption), the shortest ones for the studied family of materials. Its adsorption isotherm is free of kinetic effects (Figure 6) and the pore limit capacity (n_p) for hydrogen storage, at $P_{eq} \rightarrow \infty$, estimated from eq 2, was the largest one found in this study, close to 12 H_2 molecules per cavity (1.82 wt %) (Table 3). Excluding the case of sodium, the ordering of the studied compounds according to this parameter, n_p, is: Zn_3Co_2-R > $Zn_3K_2Fe_2$ > $Zn_3Rb_2Fe_2$ > $Zn_3Cs_2Fe_2$. This order is quite similar to that discussed above from the CO_2 adsorption data.

TABLE 3: Results Derived from the H_2 Adsorption Isotherms Fitting According to the Langmuir−Freundlich Model[a]

compd	*T*, [K]	n_p, [mol/ mol]	H_2/cavity	$P_{0.5}$, [kPa]	*g*	wt [%]
$Zn_3K_2Fe_2$	75	5.8 ± 0.3	11.6	46 ± 14	3.3 ± 0.3	1.66 ± 0.01
	85	4.5 ± 0.1	9	45 ± 3	1.8 ± 0.2	1.29 ± 0.01
$Zn_3Rb_2Fe_2$	75	4.7 ± 0.1	9.4	56 ± 3	1.8 ± 0.08	1.19 ± 0.01
	85	4.4 ± 0.2	8.8	162 ± 12	1.33 ± 0.08	1.11 ± 0.05
$Zn_3Cs_2Fe_2$	75	4.19 ± 0.04	8.4	39.6 ± 0.9	1.68 ± 0.05	0.95 ± 0.01
	85	3.52 ± 0.02	7.4	70.9 ± 0.9	1.29 ± 0.03	0.79 ± 0.01
Zn_3Co_2-R	75	5.8 ± 0.1	11.6	113 ± 5	1.17 ± 0.08	1.82 ± 0.01
	85	5.35 ± 0.05	10.7	288 ± 6	1.08 ± 0.01	1.71 ± 0.02

[a] n_p, is the limit capacity of micropores; $P_{0.5}$ is the pressure at $n_{ad} = 0{,}5.n_p$; *g* is the osmotic coefficient, H_2/cavity, is the estimated limit amount of H_2 molecules per cavity; and wt % is the maximum estimated adsorption in weight percent.

The variation for the osmotic coefficient (*g*) (Table 3) appears as a sensor for the guest−host interaction in the studied series of porous materials. For a given composition, the larger value of *g* is always observed for the adsorption isotherm recorded at the lower temperature (liquid N_2), where the stronger guest−host interaction takes place. Within the considered materials as a whole, the *g* value decreases according to K > Rb > Cs > Zn_3Co_2-R. This order parallels the above-discussed evidence for the strength of the guest−host interaction obtained from the isotherms slope at low-pressure values (Figure 7). The potentiality of the osmotic parameter (*g*) in the LF model as sensor for the guest−host interactions in porous hexacyanometalates has already observed from the evaluation of Xe adsorption data[21] and is discussed with details below.

3.5. On the Used Adsorption Models. The guest−host interactions for CO_2 and H_2 have been discussed according to parameter values derived from the adsorption data processing according to two different adsorption models, DA and LF, respectively. The LF model has a more general validity, whereas the DA one is limited to vapors. For CO_2, these parameters are the characteristic energy (E_o) and the adsorption potential (*A*), whereas in the LF model, the value for the osmotic coefficient (*g*) appears as a sensor for the interaction strength. In the DA model, the value of E_o is a function of the average energy involved in the pore filling as whole, while *A* senses the variation for the adsorption potential on the pore filling.[23] eq 2 is derived from the osmotic theory of adsorption in micropores where an "osmotic" equilibrium between two solutions (vacancies and molecules), one of them created in the micropores and the other one in the gas phase, is established.[24] In this model, the pore free volume (vacuum) represents the vacancies and behaves as the solvent while the solute is represented by the adsorbed molecules. In such a model, the value of *g* senses the interaction between these solutions (solute and solvent). For $g = 1$ eq 2 reduces to the Langmuir type-isotherm, which can be derived from statistical mechanics for a system of open and independent cavities that exchange energy and particles, assuming mobile adsorption without lateral interactions and with all of the molecules inside sensing the same energy adsorption.[36] This is equivalent to an ideal solution of vacuum plus adsorbed molecules. A value of $g > 1$ measures the deviation of such a solution from the ideal, i.e., the solute−solvent (guest−host) interaction. This explains the above-discussed experimental evidence where the value of *g* appears as a good sensor for the strength of the guest−host interaction during the hydrogen adsorption.

In order to illustrate the equivalence among the results obtained from these two models in the materials under study, the CO_2 adsorption data were evaluated also according to LF model. In Table 2, the obtained values for *g* are included. Between the values of E_o and *g* a positive correlation is noted. To a stronger guest−host interaction given by a larger E_o value, the calculated *g* value is also the larger one. For some limit cases, e.g., $n = 2$ in DA model, an analytical expression supporting that correlation has been reported.[37] In Figure 9, a plot of *g* versus E_o from the CO_2 adsorption data is presented. From low to medium values of *g*, a practically linear correlation is observed; however, a remarkable deviation of that behavior was noted as the *g* value increases. Additionally, the uncertainty for the estimated *g* value (from the nonlinear fitting) is higher as its value increases. This suggests that for a large deviation from the ideal ($g = 1$), i.e., a strong guest−host interaction, a less reliable description of the adsorption data according to the osmotic model is expected. Such a regularity has been observed by us in previous studies where LF model has been used for the adsorption data evaluation.[21,25,30]

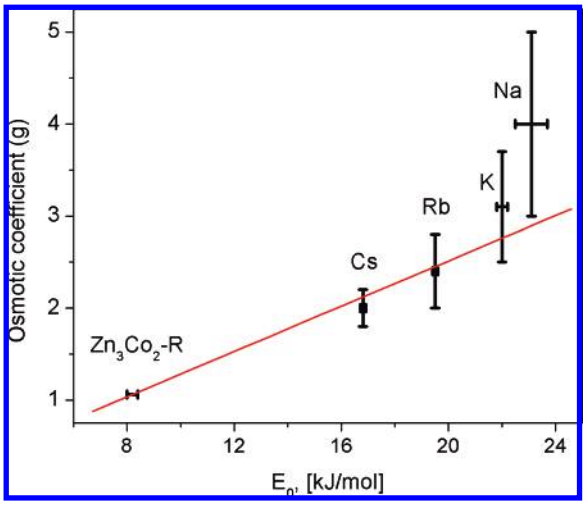

Figure 9. Plot of the osmotic coefficient (*g*) versus characteristic energy (E_o) corresponding to the CO_2 adsorption data fitting according to the LF and DA models, respectively.

3.6. Heats of Adsorption for Hydrogen. The hydrogen adsorption heats were estimated from adsorption isotherms recorded at N_2 and Ar baths. Figure 10 shows these isotherms for samples of $Zn_3K_2Fe_2$ and Zn_3Co_2-R. The smallest difference in the adsorbed amount for the two temperatures at a given pressure value corresponds to the K-containing sample revealing that the stronger guest−host interaction is involved. For Rb and Cs, the comparison of the corresponding isotherms (see Supporting Information) leads to an analogue evidence for Rb relative to Cs. If that difference for adsorbed amount at a given pressure value is taken as indicator of the guest−host interaction strength, then the order results K > Rb > Cs > Zn_3Co_2-R. This agrees with the above-discussed results from the isotherms fitting, particularly with the ordering derived from the calculated *g* values.

Figure 10 shows the variation for the adsorption heat (ΔH_{ads}) versus the amount adsorbed (n_{ads}), calculated according to eq 4 using the adsorption data collected from N_2 and Ar baths. In

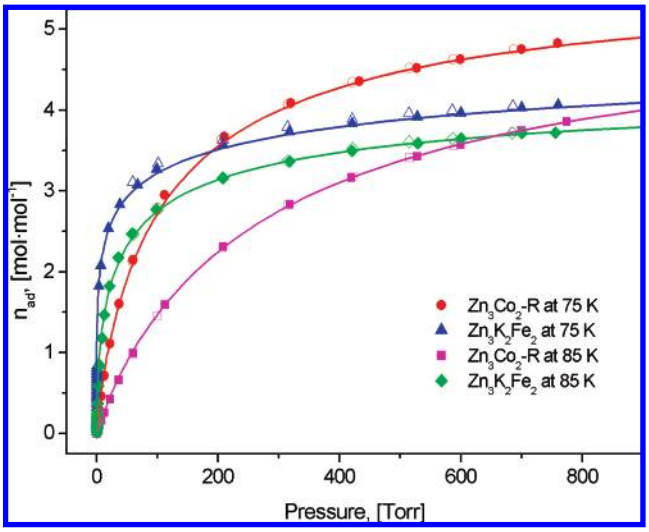

Figure 10. H_2 adsorption isotherms for Zn_3Co_2-R and $Zn_3K_2Fe_2$ recorded at 75 and 85 K using liquid N_2 and Ar baths. The stronger guest−host interaction for $Zn_3K_2Fe_2$ is appreciated as a smaller difference in the adsorbed amount for a given value of pressure.

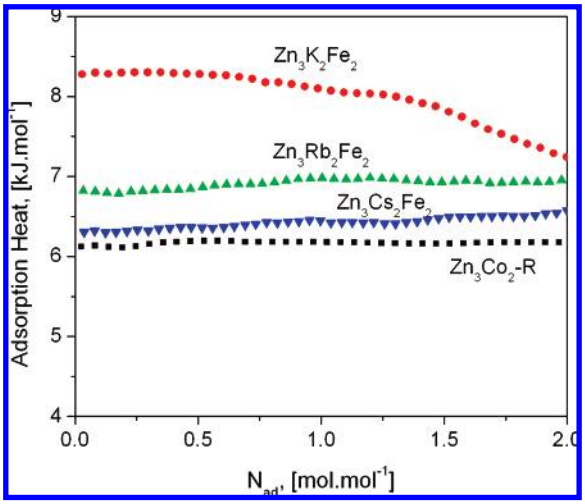

Figure 11. Hydrogen adsorption heat curves (the low adsorption region only) in the materials under study. The estimated adsorption heat follows the order K > Rb > Cs > Zn_3Co_2-R.

order to reduce the guest−guest interaction contribution to the estimated ΔH_{ads} value, only the region of low adsorption (small n_{ads} values) were considered. The obtained ΔH_{ads} values follow the order K > Rb > Cs > Zn_3Co_2-R, in correspondence with the qualitative evidence already discussed. This order represents a conclusive clue on the role of the cavity electric field gradient for hydrogen molecule stabilization within the cavity. The hydrogen adsorption in the materials under study appears to be dominated by the electrostatic interaction among the cavity electric field gradient and the adsorbate quadrupole moment. The slight positive slope observed in ΔH_{ads} vs n_{ads} curves for Rb and Cs was tentatively attributed to the metal mobility within the cavity in order to find a new equilibrium position to allow a stronger interaction with the H_2 molecule. For K, the inverse behavior was observed, probably due to a stronger interaction of this smaller and more polarizing ion with the framework surface. For Zn_3Co_2-R, the calculated ΔH_{ads} does not show variation with n_{ads}. This suggests that in this compound, due to the low electric field gradient at the cavity, the contributions of both, the guest−host and the guest−guest interactions to the hydrogen adsorption, are quite similar.

As already mentioned, the interaction of molecular hydrogen with alkali metals exchanged zeolites has been studied from quantum mechanical calculations concluding that the cations embedding in the zeolite framework causes a dramatic decrease of their polarizing power and, as a consequence, also in the predicted hydrogen adsorption heats.[4,6] However, for Mg (2+), a highly polarizing cation, the calculated value of ΔH_{ads} amounts to ∼10 kJ/mol,[6] a value only slightly higher than that here obtained for K (8.3 kJ/mol). Compared with Mg, K is a metal with less polarizing power (0.433 for K^+ vs 2.704 for Mg^{2+}).[33] This suggests that in zeolite, the interaction with the framework may effectively be shielding the metal polarizing power and its ability to favor the excess of the hydrogen molecule within the cavity. Such a shielding effect could also be present in the studied porous cyanometalates; however, their framework atoms are involved in relatively highly covalent bonds resulting in a weaker alkali metal-framework interaction and probably in a lower shielding effect.

The above-discussed experimental results for zeolite-like hexacyanometalates reveal that the electric gradient within the pores, given by the alkali metal ion, has a decisive role on the hydrogen molecule adsorption in this family of materials.

The ΔH_{ads} value obtained for K, 8.3 kJ/mol, is ∼20% higher than that reported for $Ni_3[Co(CN)_6]_2$, the Prussian blue analogue where the largest value of adsorption heat for molecular hydrogen has been estimated.[11] The ΔH_{ads} value measured for Zn_3Co_2-R, of about 6.3 kJ/mol, is similar to that reported for zinc cobalticyanide with a supposed cubic structure.[16] On dehydration by heating, cubic zinc cobalticyanide undergoes a structural transformation to form the rombohedral phase.[19]

3.7. On the Structural Changes in the Materials under Study with Adsorbed Species. In those porous cyanometalates where the H_2 adsorption has been reported,[11−16] the porous network results from systematic absence of the molecular anionic building block. From this fact, at the pore surface, we always find metal centers with an unsaturated coordination environment. In the as-prepared materials, such available coordination sites are occupied by water molecules. These coordinated waters can be removed through moderated heating, usually below 100 °C, liberating the materials free space for adsorption processes.[21,25,38] The dehydration process is always accompanied of the unit cell contraction, which amounts up to 4% for the cell volume reduction.[29,38,39] On the water removal, all of the bonding interactions of the metal sited at pore surface is with the CN groups. This leads to an increase for the charge subtraction from these groups, via σ-bonding (through 5σ orbitals), which is detected as a reduction for the T−N≡C−M−C≡N−T chain length, which coincides with the unit cell edge. This is a reversible effect. On sample re-hydration, the cell edge size is restored. For this type of porous material, the adsorption process is always accompanied of a certain cell expansion, which is more pronounced for polar species, like water, with a relatively strong interaction with the metal centers at the pore surface. However, for the series of porous hexacyanometalates here studied, the coordination sphere for the zinc atom is saturated by N atoms from CN groups. Since the −C≡N− bridge forms relatively strong bonds with the metal centers, no appreciable cell expansion on the adsorption process is expected. For Zn_3Co_2-R, the cell contraction on cooling from room temperature to 77 K, including degassing, amounts a unit cell volume reduction below 0.4%.[19] For the $Zn_3A_2Fe_2$ series, according to the above-discussed results, the guest−host interaction is dominated by the exchangeable metal (A), and such interaction probably causes the migration of the metal through

different equilibrium positions within the cavity, as already mentioned, an effect well-known for zeolites,[32] but not an appreciable unit cell expansion. A study on the cation mobility on the pore filling in this family of materials is on the way.

Conclusions

The hydrogen storage in a series of zinc hexacyanoferrates (II) with different alkali metal (Na^+, K^+, Rb^+, Cs^+) located within the porous framework was studied. The alkali metal modulates the electric field gradient within the pores and thereby also the guest−host interaction for the hydrogen molecule adsorption. The calculated adsorption heat (ΔH_{ads}) values follow the order: K > Rb > Cs > Zn_3Co_2-R. A strong electrostatic interaction within the cavity favors the hydrogen retention but it can also reduce the diffusion rate for the hydrogen molecule through narrow windows. Such an effect was observed for Na^+, the smaller and most polarizing alkali metal among the studied series. The H_2 adsorption isotherm in zinc-sodium ferrocyanide showed pronounced kinetic effects even at 258 K. For rhombohedral zinc hexacyanocobaltate (III), with a crystal structure and porous network similar to that observed for the zinc hexacyanoferrates (II) but free of alkali metal, the smallest pore filling time and the largest hydrogen storage capacity were found and with an isotherm free of kinetic effects. The low electric field gradient at the cavity surface for this material facilitates a fast hydrogen diffusion rate through the interconnected network of cavities. The CO_2 adsorption isotherms reveal that the alkali metal located close to the pore windows does not represent a limiting factor for the pore filling with small molecules. The free volume for all of the studied compositions was found to be accessible for CO_2. The pore volume, estimated from the CO_2 adsorption, follows the order: Zn_3Co_2-R > Na > K > Rb > Cs. For the estimated characteristic energy, which senses the average guest−host interaction strength, the order is as follows: Na > K, > Rb > Cs > Zn_3Co_2-R, which parallels the expected electric field gradient at the cavity. The H_2 and CO_2 adsorption in the materials under study shed light on the role of the electric field gradient at the cavities region for the hydrogen storage in porous cyanometalates.

Acknowledgment. L.R. acknowledges the support provided by the ALFA Project NANOGASTOR for her PhD studies. The help of J. Rodríguez-Hernández for the preparation of some figures and of C.P. Krap for the H_2 adsorption data collection, respectively, are highly appreciated. This research was partially supported by the Projects SEP-2004-C01-47070 and SEP-CONACyT-2007-61541. The authors thank E. Fregoso-Israel from IIM−UNAM for the TG data collection.

Supporting Information Available: Supplementary adsorption data including the H_2 isotherms recorded in both N_2 and Ar baths for Rb and Cs. This information is available free of charge via the Internet at http://pubs.acs.org.

References and Notes

(1) Kamat, P. V. *J. Phys. Chem. C* **2007**, *111*, 2834.
(2) Schlapbach, L.; Züttel, A. *Nature* **2001**, *414*, 353, and references therein
(3) Janot, R.; Eymery, J. B.; Tarascon, J. M. *J. Phys. Chem. C* **2007**, *111*, 2335.
(4) Torres, F. J.; Vitillo, J. G.; Civalleri, B.; Ricchiardi, G.; Zecchina, A. *J. Phys. Chem. C* **2007**, *111*, 2505.
(5) Bhatia, S. K.; Myers, A. L. *Langmuir* **2006**, *22*, 1688.
(6) Torres, F. J.; Civalleri, B.; Terentyev, A.; Ugliengo, P.; Pisani, C. *J. Phys. Chem. C* **2007**, *111*, 1871, and references therein.
(7) Rosi, N. L.; Eckert, J.; Eddaoudi, M.; Vodak, D. T.; Kim, J.; O'Keeffe, M.; Yaghi, O. M. *Science* **2003**, *300*, 1127.
(8) Sun, D.; Ma, S.; Ke, Y.; Collins, D. J.; Zhou, H.-C. *J. Am. Chem. Soc.* **2006**, *128*, 3896.
(9) Kaye, S. S.; Dailly, A.; Yaghi, O. M.; Long, J. R. *J. Am. Chem. Soc.* **2007**, *129*, 14176, and references therein.
(10) Vitillo, J. G.; Damin, A.; Zecchina, A.; Ricchiardi, G. *J. Chem. Phys.* **2006**, *124*, 224308.
(11) Kaye, S. S.; Long, J. R. *J. Am. Chem. Soc*. **2005**, *127*, 6506.
(12) Chapman, K. W.; Southon, P. D.; Weeks, C. L.; Kepert, C. J. *Chem. Commun*. **2005**, 3322.
(13) Hartman, M. R.; Peterson, V. K.; Liu, Y.; Kaye, S. S.; Long, J. R. *Chem. Mater.* **2006**, *18*, 3221.
(14) Culp, J. T.; Matranga, C.; Smith, M.; Bittner, E. W.; Bockrath, B. *J. Phys. Chem. B.* **2006**, *110*, 8325.
(15) Kaye, S. S.; Long, J. R. *Catal. Today* **2007**, *120*, 311.
(16) Natesakhawat, S.; Culp, J. T.; Matranga, C.; Bockrath, B. *J Phys. Chem. C* **2007**, *111*, 1055.
(17) Turnes Palomino, G.; Llop Carayol, M. R.; Otero Areán, C. *J. Mater Chem.* **2006**, *16*, 2884.
(18) Gravereau, P.; Garnier, E.; Hardy, A. *Acta Crystallogr. B* **1979**, *35*, 2843.
(19) Rodríguez-Hernández, J.; Reguera, E.; Lima, E.; Balmaseda, J.; Martínez-García, R.; Yee-Madeira, H. *J. Phys. Chem. Solids* **2007**, *68*, 1630.
(20) Martinez-García, R.; Knobel, M.; Reguera, E. *J. Phys. Chem. B* **2006**, *110*, 7296.
(21) Lima, E.; Balmaseda, J.; Reguera, E. *Langmuir* **2007**, *23*, 5752.
(22) Garnier, E.; Gravereau, P. *Rev. Chim. Mineral.* **1983**, *20*, 68.
(23) Dubinin, M. M. In *Progress in Surface Science and Membrane Science*; Cadenheat, D. A., Ed.; Academic Press: New York, 1975.
(24) Bering, B. P.; Serpinskii, V. V. *Izv. Akad. Nauk, Ser. Khim.* **1974**, *11*, 2427.
(25) Balmaseda, J.; Reguera, E.; Rodríguez-Hernández, J.; Reguera, L.; Autie, M. *Micropor. Mesopor. Mater.* **2006**, *96*, 222.
(26) Stoeckli, F. *Russ. Chem. Bull. Int. Ed.* **2001**, *50*, 2265.
(27) Rouquerol, F.; Rouquerol, J.; Sing, K. *Adsorption by Powders and Solids: Principles, Methodology and Applications*; Academic Press: London, 1999.
(28) Gravereau, P.; Garnier, E.; Hardy, A. *Acta Crystallogr. B* **1982**, *38*, 1401.
(29) Balmaseda, J.; Reguera, E.; Gomez, A.; Roque, J.; Vazquez, C.; Autie, M. *J. Phys. Chem. B* **2003**, *107*, 11360.
(30) Roque, J.; Reguera, E.; Balmaseda, J.; Rodríguez-Hernández, Reguera, L.; del Castillo, L. F. *Micropor. Mesopor. Mater.* **2007**, *103*, 57.
(31) Shannon, R. D. *Acta Crystallogr. A* **1976**, *32*, 751.
(32) Jaramillo, E.; Grey, C. P.; Auerbach, S. M. *J. Phys. Chem. B* **2001**, *105*, 12319.
(33) Zhang, Y. *Inorg. Chem.* **1982**, *21*, 3886.
(34) Krishnaji, V. P. *Rev. Modern Phys.* **1966**, *38*, 690.
(35) Rodríguez-Hernández, J.; Gómez, A.; Reguera, E. *J. Phys. D: Appl. Phys*. **2007**, *40*, 6076.
(36) Roque-Malherbe, R. In *Adsorption and Diffusion in Nanoporous Materials*; CRC Press, Taylor & Francis Group: Boca Raton, London, New York, 2007.
(37) Yakubov, T. S.; Bering, B. P.; Dubinin, M. M.; Serpinskii, V. V. *Izv. Akad. Nauk, Ser. Khim.* **1977**, 463.
(38) Gómez, A.; Rodríguez-Hernández, J.; Reguera, E. *J. Powder Diffract.* **2007**, *22*, 27.
(39) Martinez-García, R.; Knobel, M.; Reguera, E. *J. Phys.: Condens. Matter* **2006**, *18*, 11243.